



Doxorubicin-loaded amphiphilic polypeptide-based nanoparticles as an efficient drug delivery system for cancer therapy



Shixian Lv^{a,b,1}, Mingqiang Li^{a,b,1}, Zhaohui Tang^a, Wantong Song^{a,b}, Hai Sun^a, Huaiyu Liu^{c,*}, Xuesi Chen^{a,*}

^aKey Laboratory of Polymer Ecomaterials, Changchun Institute of Applied Chemistry, Chinese Academy of Sciences, Changchun 130022, China

^bUniversity of Chinese Academy of Sciences, Beijing 100039, China

^cLaboratory Animal Center, Jilin University, Changchun 130012, China

ARTICLE INFO

Article history:

Received 10 April 2013

Received in revised form 25 July 2013

Accepted 9 August 2013

Available online 17 August 2013

Keywords:

Poly(amino acids)

Doxorubicin hydrochloride

Electrostatic interaction

pH sensitive

Drug delivery

ABSTRACT

An amphiphilic anionic copolymer, methoxy poly(ethylene glycol)-*b*-poly(L-glutamic acid-co-L-phenylalanine) (mPEG-*b*-P(Glu-co-Phe)), with three functionalized domains, was synthesized and used as a nano-vehicle for cationic anticancer drug doxorubicin hydrochloride (DOX-HCl) delivery via electrostatic interactions for cancer treatment. The three domains displayed distinct functions: PEG block chain for prolonged circulation; poly(phenylalanine) domain for stabilizing the nanoparticle construct through hydrophobic/aromatic interactions; and the poly(glutamic acid) domain for providing electrostatic interactions with the cationic drug to be loaded. The copolymer could self-assemble into micellar-type nanoparticles, and DOX was successfully loaded into the interior of nanoparticles by simple mixing of DOX-HCl and the copolymer in the aqueous phase. DOX-loaded mPEG-*b*-P(Glu-co-Phe) nanoparticles (DOX-NP) had a superior drug-loading content (DLC) (21.7%), a high loading efficiency (almost 98%) and a pH-triggered release of DOX. The size of DOX-NP was ~140 nm, as determined by dynamic light scattering measurements and transmission electron microscopy. In vitro assays showed that DOX-NP exhibited higher cell proliferation inhibition and higher cell uptake in A549 cell lines compared with free DOX-HCl. Maximum tolerated dose (MTD) studies showed that DOX-NP demonstrated an excellent safety profile with a significantly higher MTD (15 mg DOX kg⁻¹) than that of free DOX-HCl (5 mg DOX kg⁻¹). The in vivo studies on the subcutaneous non-small cell lung cancer (A549) xenograft nude mice model confirmed that DOX-NP showed significant antitumor activity and reduced side effects, and then enhanced tumor accumulation as a result of the prolonged circulation in blood and the enhanced permeation and retention effect, compared with free DOX, indicating its great potential for cancer therapy.

© 2013 Acta Materialia Inc. Published by Elsevier Ltd. All rights reserved.

Introduction

Cancer is one of the most common causes of death in the world. Despite tremendous advances in cancer diagnosis and treatment, the cure for cancer is still a Gordian knot [1]. Chemotherapy remains the primary treatment for cancer among conventional modalities. However, many chemotherapeutic agents, such as cytotoxic drugs, can freely diffuse in both normal and neoplastic cells. This induces non-specific drug distribution in the body and severe systemic side effects, and therefore chemotherapy often results in an unsatisfactory curative effect due to the side effects of the drugs [2,3]. Nanosized drug carriers using natural or artificial polymers appear to be a promising and reliable approach to cancer treatment, with enhanced antitumor efficacy and reduced toxic side effects [4]. Compared with conventional systemic

chemotherapies, nanosized anticancer carriers have favorable properties based on well-preprogrammed structures, such as high drug-loading capacity, high stability by avoiding rapid clearance by the renal and reticuloendothelial systems (RES) and minimized drug loss during blood circulation [5], enhanced accumulation in tumors through the enhanced permeability and retention (EPR) effect [6] and facilitated drug release triggered by environmental stimuli in the tumor sites (e.g., temperature [7–9], pH [10–12] and glutathione [13,14]). Several nanomedicines have been approved for clinical use, such as Doxil and Abraxane, which have been used as effective treatments for metastatic breast cancer and recurrent ovarian cancer [15,16].

Among all the nanosized drug carriers, self-assembled polymeric nanoparticles of poly(ethylene glycol)-*b*-poly(amino acids) (PEG-PAA) have emerged as one of the most promising platforms for improved antitumor drug delivery and have been widely studied in preclinical and clinical trials, owing to their excellent biodegradability and biocompatibility [17]. These self-assembled nanoparticles consist of a hydrophilic PEG shell and a PAA core

* Corresponding authors. Tel./fax: +86 431 85262112 (X. Chen).

E-mail addresses: liuhuaiyu@jlu.edu.cn (H. Liu), xschen@ciac.ac.cn (X. Chen).

¹ These authors contributed equally to this paper.

incorporating antitumor drugs. The PEG shell can prevent nanoparticles from adsorption of protein and recognition by the phagocytic system, and in that way, prolong blood circulation time [5,18]. PAA is highly biocompatible, biodegradable and non-toxic, and can easily be synthesized by a well-established ring-opening polymerization (ROP) method. In addition, PAA has versatile functional groups such as carboxyl, amino, hydroxyl and thiol groups, which offer great benefits in modifying the chemical structure of the core for efficient drug incorporation and controllable drug release properties [19–22]. Accordingly, several polymeric nanoparticles of PEG-PAA incorporating doxorubicin, paclitaxel, SN-38 and cisplatin exhibited significant antitumor efficacy with appreciably lowered toxicity compared with free drugs, and are currently under clinical evaluation [23–26].

However, most of these nanomedicines are achieved by chemical conjugation and/or physical entrapment of hydrophobic drugs into the nanoparticles. The nanosized drug delivery systems based on electrostatic PEG-PAA block copolymers and the charged hydrophilic antitumor drugs are still rarely investigated. Previously, the present authors prepared a ionomer complex formed by anionic methoxy poly(ethylene glycol)-*b*-poly(L-glutamic acid) (mPEG-*b*-PLG) and cationic DOX-HCl in the therapy of non-small-cell lung cancer (NSCLC) [27]. The results demonstrated that mPEG-*b*-PLG was an efficient carrier for delivering DOX into solid tumors and achieved improved pharmacokinetics, biodistribution and then reduced toxicity compared with free DOX-HCl. However, both PEG and PLG segments of the block copolymer are hydrophilic in a physiological environment, and there are no other groups to stabilize the complex formulation; therefore, the DOX-loaded mPEG-*b*-PLG system revealed unsatisfactory cellular uptake and lower cell proliferation inhibition activity compared with free DOX-HCl. Recent studies confirmed that the stability of the nanoparticles was a key factor for a successful drug delivery system [28,29]. By increasing the overall hydrophobicity of the block copolymer in the nanoparticles, the uptake of the drug carriers by the tumor cells can be greatly enhanced, which will lead to a significant increase in anticancer activity.

Herein, a drug delivery system is developed based on PEG-PAA loaded with hydrophilic DOX-HCl. As an anionic polymer to facilitate self-assembled nanoparticle formation via electrostatic interactions with DOX, a novel A(BC) copolymer composed of three monomeric units, mPEG-*b*-P(Glu-*co*-Phe), is used. Amphiphilic anionic mPEG-*b*-P(Glu-*co*-Phe) block copolymers are expected to undergo spontaneous self-assembly in aqueous solutions, and three monomeric units of the copolymer are expected to perform specified functions for efficient drug delivery. PEG is used for the prolonged circulation of nanoparticles for effective EPR effects. Anionic poly (glutamic acid) serves as the functional group of the copolymer to provide the electrostatic interaction with cationic DOX-HCl. The incorporation of phenylalanine units into the copolymer is considered to enhance hydrophobic/aromatic interactions within the nanoparticle core.

Compared with other types of nanoparticles and microparticles for drug delivery, the present nanoparticles have the following advantages. (1) Most of the reported drug-loaded nanocarriers are obtained through hydrophobic drug encapsulation procedures, which involve the dissolution of the polymeric carrier and drug in an organic solvent and the subsequent removal of the organic solvent by either dialysis or solvent evaporation. For example, DOX-HCl is usually neutralized by excess triethylamine and makes doxorubicin hydrophobic in organic solvents (*N,N*-dimethylformamide (DMF), tetrahydrofuran, chloroform or dimethylsulfoxide (DMSO)). Nevertheless, the trace residual triethylamine and solvent may do harm to the human body. Conversely, the present mPEG-*b*-P(Glu-*co*-Phe)/DOX polyion complex nanoparticles can be prepared by simple mixing of the drug and the copolymers in

aqueous solution, without the use of harmful organic solvents. This approach will make the drug encapsulation procedure much simpler and safer. Additionally, electrostatic interactions between the polymers and the drugs would offer great benefits for drug release. Since the environmental acidity has a great impact on the surface charge of the electrostatic block copolymers and also affects electronic interactions between the polymers and the drugs, such electrostatic polymer/drug complexes could be designed for intracellular pH-sensitive drug delivery systems [30–32]. (2) Compared with other electrostatic polymer/drug polyion complex nanoparticles, the present nanoparticles also have advantages. Unlike most of the reported anionic polymer/DOX-HCl complexes, which were based on non-biodegradable polymers (e.g., poly(methacrylic acid) and poly(acrylic acid)) and devoid of *in vivo* studies [33,34], the design of the present system is based on biocompatible and biodegradable PEG-PAA. Compared with other biodegradable polymers (e.g., γ -polyglutamic acid and poly(ethylene glycol)-*b*-poly(L-glutamic acid) [27,32], hydrophobic groups were introduced into the copolymers to enhance the construct stability of the nanoparticles towards dissociation by a simple copolymerization procedure of γ -benzyl-L-glutamate-*N*-carboxyanhydride (BLG-NCA) and Phe-NCA monomers. Additionally, incorporation of phenylalanine units into the copolymer was also expected to enhance the cell uptake of DOX-NP, which could enhance the overall therapeutic efficacy.

In the present work, the molecular structures, physicochemical properties, self-assembly, stability and loading capacity of mPEG-*b*-P(Glu-*co*-Phe) block copolymer were assessed. The *in vitro* drug release kinetics, cellular uptake and *in vitro* cytotoxicity of DOX-NP were further studied. Finally, the antitumor efficacy of DOX-NP in a NSCLC (A549) xenograft model was evaluated. The DOX-loaded electrostatic complex nanoparticles showed reduced systemic toxicity and enhanced antitumor efficacy compared with free DOX-HCl, indicating its great potential for efficient cancer chemotherapy.

2. Experimental section

2.1. Materials

Poly(ethylene glycol) monomethyl ether (mPEG, $M_n = 5000$) was purchased from Aldrich and used without further purification. BLG-NCA and amino-terminated poly(ethylene glycol) methyl ether (mPEG-NH₂, $M_w = 5000$ Da) were synthesized as in previous work [35]. L-Phenylalanine-*N*-carboxyanhydride (Phe-NCA, 98%; Shanghai Yeexin Biochem&tech Co., Ltd.) was recrystallized from *n*-hexane/tetrahydrofuran (1:1) before use. DMF was stored over calcium hydride (CaH₂) and purified by vacuum distillation with CaH₂. Doxorubicin hydrochloride (DOX-HCl) was purchased from Beijing Huafeng United Technology Corporation. 3-(4,5-Dimethylthiazol-2-yl)-2,5-diphenyl tetrazolium bromide (MTT) and 4',6-diamidino-2-phenylindole dihydrochloride (DAPI) were purchased from Sigma and used as received. All the other reagents and solvents were purchased from Sinopharm Chemical Reagent Co. Ltd. and used as received.

2.2. Characterization

¹H NMR spectra were recorded on a Bruker AV 400 NMR spectrometer in trifluoroacetic acid-*d* (CF₃COOD). Number- and weight-average molecular weights (M_w , M_n), and molecular weight distributions (PDI = M_w/M_n) were determined by gel permeation chromatography (GPC) using a Waters GPC system (Waters Styragel HT6E column, with OPTILAB DSP interferometric refractometer as the detector). The eluent was DMF containing 0.01 M lithium

bromide (LiBr) at a flow rate of 1.0 ml min⁻¹ at 40 °C. Monodispersed polystyrene and poly(ethylene glycol) with different molecular weights were used to generate the calibration curves. Dynamic laser scattering (DLS) measurements were performed on a WyattQELS instrument with a vertically polarized He–Ne laser (DAWN EOS, Wyatt Technology) at 90° collecting optics. Zeta-potentials were measured with a Zeta Potential/BI-90 Plus particle size analyzer (Brookhaven, USA) at room temperature. Transmission electron microscopy (TEM) measurement was performed on a JEOL JEM-1011 transmission electron microscope with an accelerating voltage of 100 kV. A drop of the micelle solution (0.1 mg ml⁻¹) was deposited onto a 230 mesh copper grid coated with carbon and allowed to dry in air at 25 °C before measurements. Critical micelle concentration (CMC) was measured by fluorescence spectroscopy using pyrene as a probe on a Perkin-Elmer LS50B luminescence spectrometer with an emission wavelength of 390 nm. The excitation fluorescence at 339 and 335 nm was monitored. CMC was estimated as the cross-point of the tangent to the horizontal line of I_{339}/I_{335} with the relative constant values and the diagonal line with rapidly increased I_{335}/I_{332} ratio. UV–Vis and fluorescence spectra were measured on a UV-2401PC spectrophotometer (SHIMADZU) and a fluorescence spectrometer (LS50B, Perkin Elmer), respectively.

2.3. Synthesis of mPEG-*b*-P(BLG-*co*-Phe) copolymers

mPEG-*b*-P(BLG-*co*-Phe) was synthesized by ROP in DMF using mPEG-NH₂ as initiator. In brief, after mPEG-NH₂ (4 g, 0.8 mmol) in a 250-ml glass reactor was used and after an azeotropic dehydration process with toluene, BLG-NCA (2.104 g, 8 mmol) and Phe-NCA (1.529 g, 8 mmol) were added, then dry DMF (80 ml) was injected via a syringe. After stirring for 3 days at 35 °C, the mixture was precipitated into an excess amount of ice diethyl ether to give mPEG-*b*-P(BLG-*co*-Phe) block copolymers. The purified product was dried under vacuum at room temperature for 48 h. Yield: 89.9%. ¹H NMR (400 MHz, TFA-d, ppm): δ 3.67 (PEG chain), 6.82–7.01 (C₆H₅-), 2.78 (C₆H₅-CH₂- of polyphenylalanine), 4.95 (C₆H₅-CH₂- of γ-benzyl groups), 4.48–4.59 (CH of amide of polyglutamic acid and polyphenylalanine), 1.85–1.95 (-CH₂-CH₂-CO-), 2.26 (-CH₂-CH₂-CO-).

2.4. Synthesis of mPEG-*b*-P(Glu-*co*-Phe) copolymers

In order to remove the protecting group, mPEG-P(BLG-Phe) (2 g) was dissolved in dichloroacetic acid (20 ml) and HBr/acetic acid (33 wt.%, 6 ml) was added. After stirring for 1 h at 35 °C, the mixture was precipitated into excessive ice diethyl ether. After drying under vacuum, the precipitate was dissolved in DMF and dialyzed against distilled water, and then freeze-dried to give mPEG-*b*-P(Glu-*co*-Phe) product. Yield: 81.0%. ¹H NMR (400 MHz, TFA-d, ppm): δ 3.67 (PEG chain), 6.82–7.11 (C₆H₅-CH₂-), 2.78 (C₆H₅-CH₂- of polyphenylalanine), 4.38–4.66 (CH of amide of poly(glutamic acid) and polyphenylalanine), 1.75–2.01 (-CH₂-CH₂-COOH), 2.31 (-CH₂-CH₂-COOH).

2.5. Preparation of DOX-loaded nanoparticles and in vitro DOX release study

mPEG-*b*-P(Glu-*co*-Phe) was dissolved in distilled water and adjusted to pH 7.0–7.5 by adding 0.1 M NaOH solution, then DOX-HCl dissolved in distilled water was added to the solution dropwise. After stirring overnight, free DOX-HCl was removed by dialysis, using a dialysis bag (MWCO 3500 Da) against deionized water for 24 h, and then freeze-dried to obtain DOX-NP. DOX loaded inside the nanoparticles was determined by UV absorption at 480 nm.

The DLC (wt.%) and the drug-loading efficiency (DLE, wt.%) of DOX-NP were calculated by the following equations:

$$\text{DLC}\% = \frac{\text{amount of DOX in nanoparticles}}{\text{amount of DOX - loaded nanoparticles}} \times 100\%$$

$$\text{DLE}\% = \frac{\text{amount of DOX in nanoparticles}}{\text{amount of DOX used for nanoparticles preparation}} \times 100\%$$

For the drug release study, 2 mg freeze-dried DOX-NP was resuspended in 10 ml phosphate buffered saline (PBS) solution at different pH (7.4, 6.8 and 5.5). The samples were sealed in dialysis bags (MWCO 3500 Da) and incubated in the release media (40 ml) at 37 °C with a shaking rate of 100 rpm. At a predetermined time, 4 ml of incubated solution was taken out and replaced with fresh PBS. The released amount of DOX was determined by measuring the emission fluorescence intensity at 590 nm with an excitation wavelength of 490 nm.

2.6. Cell lines and culture conditions

HeLa (Human cervical carcinoma) cells and A549 (human pulmonary carcinoma) cells were cultured in Dulbecco's modified Eagle's medium (DMEM) with high glucose containing 10% fetal bovine serum, supplemented with 50 U ml⁻¹ penicillin and 50 U ml⁻¹ streptomycin, and incubated at 37 °C in a 5% CO₂ atmosphere.

2.7. In vitro cytotoxicity assay and cell uptake

The in vitro cytotoxicity was assessed with a MTT viability assay against HeLa and A549 cells. HeLa or A549 cells were seeded in 96-well plates at 10,000 cells per well in 100 μl DMEM medium and incubated for 24 h, followed by removal of the culture medium and addition of mPEG-*b*-P(Glu-*co*-Phe), DOX, DOX-NP (200 μl in complete DMEM medium) at the different concentrations. The cells were subjected to MTT assay after being incubated for another 24 h or 48 h. At the end of the experiments, 20 μl of MTT solution (5 mg ml⁻¹ in PBS) was added to each well. The plate was returned to the incubator. After 4 h, the MTT solution was carefully removed from each well, and the MTT-formazan generated by live cells was dissolved in 200 μl DMSO. The absorbance of the solution was measured on a Bio-Rad 680 microplate reader at 492 nm. Cell viability (%) was calculated by $(A_{\text{sample}}/A_{\text{control}}) \times 100$, where A_{sample} and A_{control} denote absorbance of the sample well and control well, respectively. Data are presented as average ± SD ($n = 3$).

The cellular uptake experiments were performed using flow cytometry and confocal laser scanning microscopy (CLSM). For CLSM studies, A549 cells were seeded onto glass coverslips placed in six-well plates at 1×10^5 cells per well and incubated for 24 h to ensure cell adhesion, and then treated with free DOX and DOX-NP (DOX concentration = 5 μg ml⁻¹) for 1 and 3 h. Then, the cells were washed three times with PBS and fixed with fresh 4% paraformaldehyde for 30 min at room temperature. The cell nuclei were stained with DAPI, following the manufacturer's instructions. The coverslips were placed onto the glass microscope slides, and DOX uptake was visualized using a CLSM (Carl Zeiss LSM 700).

For the flow cytometry, A549 cells were seeded in 6-well plates at 2×10^5 cells per well and incubated for 24 h, and then treated with free DOX and DOX-NP (DOX concentration = 5 μg ml⁻¹) for 1 and 3 h. Thereafter, the cells were harvested and washed three times with PBS. DOX uptake was obtained using a FACS Aria flow cytometer (BD Biosciences, CA, USA). For each sample, a minimum of 1×10^4 cells was collected for analyzing the DOX fluorescence intensity.

2.8. Apoptotic analysis

The cytotoxic effects of free DOX and DOX-NP on A549 cells were determined by fluorescent-activated cell sorting (FACS) using propidium iodide (PI) and annexin V staining. Briefly, A549 cells were seeded in 6-well plates at 2×10^5 cells per well and incubated for 24 h, and then treated with free DOX and DOX-NP (DOX concentration = $1 \mu\text{g ml}^{-1}$) for 24 h. The cells were treated with an Annexin V-FITC apoptosis detection kit (KeyGEN Biotech, China) following the manufacturer's instructions. The apoptotic activities of the free DOX and DOX-NP were performed using flow cytometry in the same manner.

2.9. Animal use

Male BALB/c nude mice (6–8 weeks old) were purchased from the Experimental Animal Center, Chinese Academy of Sciences (Shanghai, China). Kunming mice (6–8 weeks old, male) were purchased from Laboratory Animal Center, Jilin University (Changchun, China). All the animals used in this study were maintained under the required conditions in accordance with guidelines evaluated (e.g., pathogen-free condition for nude mice, free access to food and water) and approved by the Animal Care and Use Committee of Jilin University.

2.10. MTD

The Kunming mice were divided into 10 groups ($n = 3$) and administered intravenously with the free DOX or DOX-NP (5, 10, 15, 20, 25 mg DOX kg^{-1} body weight) for a single dose. Changes in body weight and survival of mice were measured daily for 10 days. The MTD was defined as the dose that causes neither mouse death due to the toxicity nor >15% of body weight loss or other remarkable changes in the general appearance within the entire period of the experiments.

2.11. Excised imaging

The A549 tumor-bearing BALB/c nude mice were injected with DOX and DOX-NP in a volume of 0.1 ml/10 g body weight via the tail vein, at a dose of 5 mg kg^{-1} (DOX equivalent). After the injection, mice were sacrificed at 2 and 10 h, and the tumor and major organs (heart, kidney, liver, lung and spleen) were collected. After rinsing with PBS three times, the excised organs were visualized using the Maestro In Vivo Imaging System (Cambridge Research & Instrumentation, Inc., Woburn, MA, USA) at excitation and emission wavelengths of 523 and 560 nm, respectively.

2.12. In vivo antitumor efficiency

The antitumor efficacy was evaluated in the human NSCLC xenograft BALB/c nude mice model. The mice were randomly divided into five groups ($n = 6$), and the freshly harvested A549 cells (1.5×10^6 cells mouse $^{-1}$; 100 μl injection $^{-1}$) were injected into the right flank of each mouse. When the tumors grew to $\sim 50 \text{ mm}^3$, the mice were randomly divided into five groups, and this day was designated as day 0. Five groups of mice were treated with the following treatments: (1) PBS (control group); (2) free DOX at 2 mg kg^{-1} ; (3) free DOX at 4 mg kg^{-1} ; (4) DOX-NP (2 mg DOX kg^{-1}); (5) DOX-NP (4 mg DOX kg^{-1}). The mice were injected intravenously four times via the tail vein at day 0, 3, 7, 10. The antitumor activity was evaluated in terms of the tumor volumes, which was calculated using the following equation: $V = a \times b^2/2$, where a and b are major and minor axes of the tumors measured by a caliper, respectively. The body weight was measured simultaneously as an indicator of the systemic toxicity.

2.13. Histopathological and immunohistochemical evaluations

The histopathological damage evaluation was assessed by the hematoxylin and eosin (H&E) method. Briefly, on day 17, the mice were anesthetized, the chests were cut open, and PBS and 4% PBS buffered paraformaldehyde were perfused from the left atrium. Tumors were collected, embedded in paraffin, and cut in 5 μm slices. The paraffin-embedded tumor slices were stained with the H&E to assess histological alterations by microscope (Nikon TE2000U).

The immunohistochemical evaluation was performed as described previously [36–38]. Rabbit monoclonal primary antibody for cleaved poly-ADP-ribose polymerase (PARP) (Abcam, Cambridge, MA, USA) and a PV-6000 two-step immunohistochemistry kit (polymer detection system for immunohistological staining; Zhongshan Goldbridge Biotechnology, Beijing, China) were used in this study.

2.14. In situ terminal deoxynucleotidyl transferase-mediated UTP end labeling (TUNEL) assay

The paraffin-embedded tumor slices were prepared as described above in the histopathological evaluation. The TUNEL assay was performed using a FragELTM DNA fragment detection kit (colorimetric-TdT Enzyme method) according to the manufacturer's protocol (EMD Chemicals Inc., Darmstadt, Germany) with minor modification (in brief, hematoxylin was used as a counterstain to replace methyl green).

2.15. Data analysis

Data are presented as mean \pm SD. Statistical significance was analyzed using Student's t -test. A p value < 0.05 was considered statistically significant.

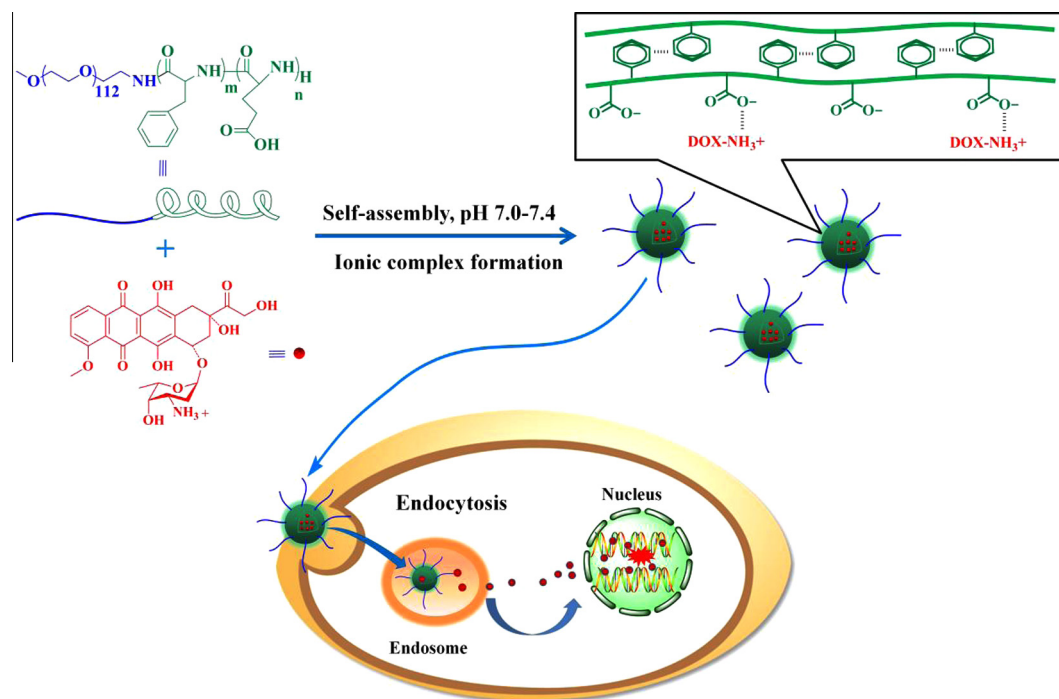
3. Results and discussion

3.1. Preparation of DOX-loaded mPEG-*b*-P(Glu-co-Phe) nanoparticles

The preparation strategy for DOX-NP is shown in Scheme 1. First, mPEG-*b*-P(Glu-co-Phe) copolymer was synthesized. Then DOX was loaded into mPEG-*b*-P(Glu-co-Phe) nanoparticles via electrostatic interaction.

mPEG-*b*-P(Glu-co-Phe) block copolymer was prepared by the one-pot ROP of BLG-NCA and Phe-NCA, using mPEG-NH₂ as the initiator, and a subsequent deprotection process of γ -benzyl in HBr/acetic acid. The ¹H NMR spectra of mPEG-*b*-P(BLG-co-Phe) and mPEG-*b*-P(Glu-co-Phe) are shown in Fig. 1. The resonances at δ 3.67 (Fig. 1B) are attributed to the methylene protons of mPEG chain ($-\text{CH}_2\text{CH}_2-$). The resonances at δ 4.38–4.66 ppm (Fig. 1C and D) are assigned to the protons of the poly (ι -glutamic acid-co-phenylalanine) backbone. The resonances at δ 6.82–7.11 ppm (Fig. 1I and J) are attributed to the phenyl protons of P(Glu-co-Phe). The resonances at δ 4.95 ppm (Fig. 1G) disappear in mPEG-*b*-P(Glu-co-Phe), which indicates the complete deprotection of the γ -benzyl groups. The molar composition ratio of the monomeric repeating units in PEG, P(Glu) and P(Phe) determined by ¹H NMR was 113:10:10, and the conversion of both monomeric BLG and Phe to polymeric P(Glu-co-Phe) was 90.9%. M_n of mPEG-*b*-P(Glu-co-Phe), calculated by ¹H NMR, was 7760 g mol $^{-1}$. GPC analyses showed that mPEG-*b*-P(BLG-Phe) copolymer had a narrow molecular weight distribution (PDI = 1.1).

The loading of DOX into mPEG-*b*-P(Glu-co-Phe) nanoparticles was performed using a very simple method under organic solvent-free conditions. As DOX is a weak amphipathic base ($\text{p}K_a = 8.3$), most of the amino groups of DOX are protonated under



Scheme 1. Schematic illustration of the preparation and the interaction mechanism of DOX-NP.

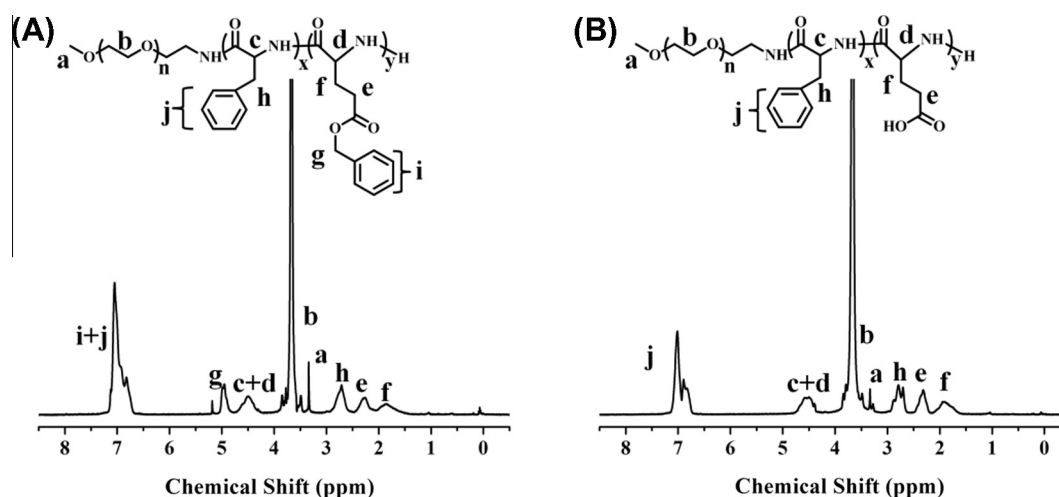


Fig. 1. ¹H NMR spectra of (A) mPEG-*b*-P(BLG-*co*-Phe) and (B) mPEG-*b*-P(Glu-*co*-Phe) in CF₃COOD.

normal physiological conditions. For loading of DOX, mPEG-*b*-P(Glu-*co*-Phe) was first dissolved in distilled water, and carboxyl groups were changed to carboxylate groups by adding NaOH solution. The drug-loading potential of mPEG-*b*-P(Glu-*co*-Phe) was investigated by spectrophotometry. As listed in Table 1, when the drug feeding ratio was ~22%, DOX-NP gave a high DOX loading content of 21.7% and a high DOX loading efficiency of ~97%, indicating that mPEG-*b*-P(Glu-*co*-Phe) nanoparticles had excellent drug-loading capacity for DOX via the electrostatic interaction between cationic DOX and anionic carriers. A higher drug-feeding ratio generated slightly higher DLC, while the DLE was remarkably reduced as a consequence. At a polymer/DOX ratio of 15/10, which is around the charge stoichiometry glutamate/doxorubicin, the DLC and DLE of DOX-NP were 25.1% and 62.7%, respectively. And a further increase in the drug feeding ratio resulted in similar DLC and lower DLE. The result demonstrated that the drug-loading

Table 1
Investigation in DLC and DLE of DOX-NP.

	Feed ratio (w/w) (polymer:DOX)	Designed DLC (%)	Measured DLC (%)	DLE (%)
1	40:11.5	22.3	21.7	97.3
2	15:10	40.0	25.1	62.7
3	10:10	50.0	26.1	52.2

capacity of mPEG-*b*-P(Glu-*co*-Phe) was ~26%. According to the literature, DLC ranging from 1% to 20% was acceptable for a polymeric drug delivery system [39]. Next, DOX-NP with DLC of 21.7% was applied in the following experiments in order to obtain a rational DLC, while maintaining higher DLE.

3.2. Solution behavior

mPEG-*b*-P(Glu-co-Phe) copolymer could self-assemble into micellar-type nanoparticles in the aqueous phase. The self-assembly behavior of the blank nanoparticles (BNP) and DOX-NP in aqueous solution was studied for CMC, zeta potential and particle size (Fig. 2). The incorporation of phenylalanine units into the copolymer was considered to enhance the construct stability in the aqueous phase through aromatic/hydrophobic interactions within the nanoparticles' inner core [21]. Pyrene was used as the fluorescence probe, and the CMC was obtained from the plot of fluorescence intensity ratio of I_{339}/I_{335} vs. $\log_{10}C$ of mPEG-*b*-P(Glu-co-Phe). The CMC value of mPEG-*b*-P(Glu-co-Phe) was determined to be $0.0207 \text{ mg ml}^{-1}$ (Fig. 2A). CMC value of the mPEG-*b*-P(Glu-co-Phe) copolymer applied in this work was comparable with those of related polymers reported in the literature [21,40]. DLS technology was used to determine the size distribution of the nanoparticles. Fig. 2 showed the results of the DLS measurement of the nanoparticles in 0.2 mg ml^{-1} . The hydrodynamic radii (R_h) of the BNP and DOX-NP were measured as 59.6 ± 13.7 and $70.2 \pm 14.2 \text{ nm}$, respectively. TEM images showed that both BNP and DOX-NP aggregated to the uniformly spherical morphology in a neutral environment with a narrow size distribution close to that determined by DLS (Fig. 2C and D).

The zeta potential of the nanoparticles was measured as shown in Fig. 2B. Owing to the pendant carboxylic acid groups of the glutamic acid units, mPEG-*b*-P(Glu-co-Phe) copolymer was negative charged at the neutral environment. For the BNP, the zeta potential was $-23.34 \pm 3.12 \text{ mV}$, while after DOX loading, it increased to $-15.76 \pm 1.49 \text{ mV}$. It has been reported that negatively charged carriers have shown potential for protein resistance and exhibited a prolonged blood circulation time for in vivo applications [41]. The zeta potential of the mPEG-*b*-P(Glu-co-Phe) copolymer under different pH conditions was also measured to evaluate the effect of

pH on the surface charge change of mPEG-*b*-P(Glu-co-Phe) nanoparticles. The results are shown in Fig. 2B. As pH decreased from 7.5 to 5.3, the zeta potential of the mPEG-*b*-P(Glu-co-Phe) nanoparticles increased from $-23.34 \pm 3.12 \text{ mV}$ to $-4.59 \pm 1.03 \text{ mV}$. The results indicate that, when the pH value changed from neutral conditions to a more acidic environment (endosomes or lysosomes), most of the negative charged carboxylate groups of glutamic acid units in mPEG-*b*-P(Glu-co-Phe) copolymer were converted to uncharged carboxyl groups; this might contribute to enhanced release of DOX from the nanoparticles intracellularly.

3.3. In vitro release of DOX

The release of DOX from mPEG-*b*-P(Glu-co-Phe) nanoparticles was investigated using a dialysis method at 37°C in PBS with varying pH values (7.4, 6.8, 5.5), as shown in Fig. 3. The release profile of DOX displayed a biphasic pattern, which was characterized by at first fast release followed by much slower release. At different pH conditions, the DOX release reached a plateau at a similar incubation time ($\sim 12 \text{ h}$), which could also be observed in other electrostatic polymer/DOX polyion complex systems [27,32,42]. The present authors inferred that the protonation of the carboxyl groups in mPEG-*b*-P(Glu-co-Phe) at different pH conditions soon reached a balance, and so did the electrostatic interaction between cationic DOX and anionic carriers, which contributed to a similar release plateau time. This study also clearly showed that the pH value of the medium had a remarkable effect on the DOX release rate from mPEG-*b*-P(Glu-co-Phe) nanoparticles. At pH 7.4, only 22% of total drug released before the release profile had virtually plateaued. This result suggests that DOX-NP maintained strong drug-polymer electrostatic interactions under physiological conditions. At pH 6.8, $\sim 29\%$ of DOX was released after 12 h. However, $\sim 60\%$ of DOX was released within 12 h when pH was decreased to 5.5. And in the end, total drug release quantity at pH 5.5 was

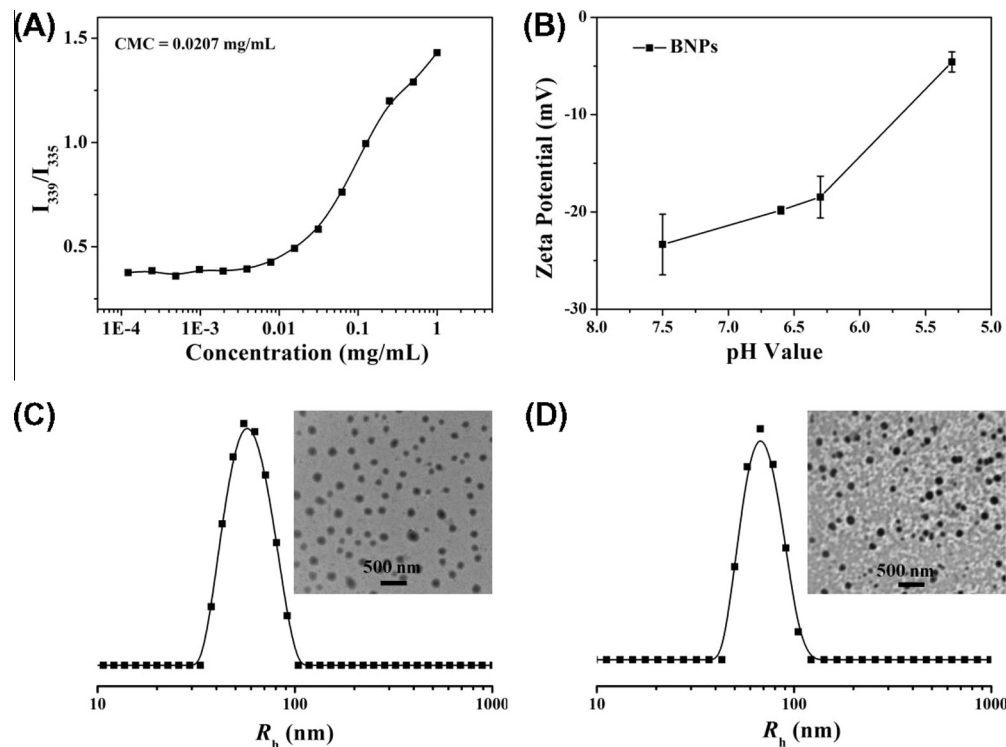


Fig. 2. Characterizations of mPEG-*b*-P(Glu-co-Phe) BNP and DOX-NP. (A) Dependence of excitation fluorescence intensity ratio of pyrene (I_{339}/I_{335}) on the logarithmic concentration of BNP. (B) Zeta-potential of BNP at different pH values; each point was an average of six measurements. (C, D) Hydrodynamic radius distribution and typical morphology of BNP and DOX-NP in aqueous solution estimated by DLS and TEM, respectively.

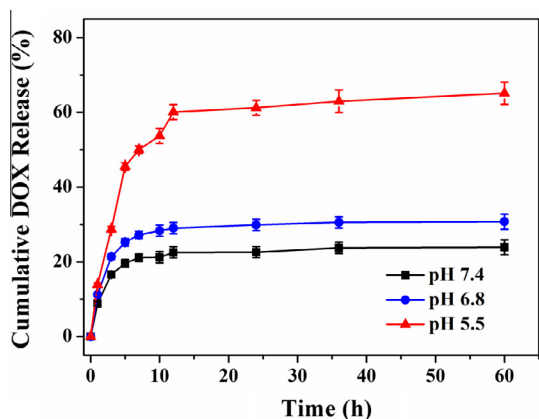


Fig. 3. DOX release profiles of the DOX-NP in PBS at various pH values (7.4, 6.8 and 5.5) at 37 °C. Each point was an average of three measurements.

approximately three times that at pH 7.4. This result demonstrated that the release of DOX from mPEG-*b*-P(Glu-*co*-Phe) nanoparticles was pH sensitive. On the basis of the aforementioned results, DOX was loaded into mPEG-*b*-P(Glu-*co*-Phe) nanoparticles by electrostatic interactions, and the degree of protonation of the carboxyl groups in mPEG-*b*-P(Glu-*co*-Phe) polymer was governed by environmental pH, after most of the carboxyl groups in mPEG-*b*-P(Glu-*co*-Phe) were protonated in low pH environment, the electrostatic interaction between mPEG-*b*-P(Glu-*co*-Phe) and DOX was weakened, and hydrophilic DOX was therefore squeezed out from the nanoparticles' inner core. However, the release did not reach 100% in the test duration, even at pH 5.5, which might be attributed to the electrostatic interaction between DOX and residual ionized carboxyl groups. Additionally, stable nanoparticles enhance construct towards dissociation, and hydrophobic

interactions between DOX and mPEG-*b*-P(Glu-*co*-Phe) polymers or DOX molecules themselves might also contribute to incomplete drug release.

The pH responsiveness is one of the most frequently used biological stimuli exploited for triggered drug release, because pH values vary in the different biological compartments and the cellular organelles. For example, the pH value at the tumor extracellular environment is more acidic (pH \approx 6.8) than that in blood (pH \approx 7.4), and the pH values in the endosomes and lysosomes are even lower (<5.5). The pH-sensitive drug carriers not only greatly reduce the side effects to normal tissues in blood circulation by minimizing drug loss, but also undergo fast release during the endocytosis process after take-up by the tumor cells, which could improve the overall therapeutic efficacy.

3.4. Cell uptake and in vitro cytotoxicity

Flow cytometry analysis was performed to compare the endocytosis of free DOX and DOX-loaded nanoparticles using A549 cells. Since DOX itself is fluorescent, it was used directly to investigate cellular uptake without additional markers. Flow cytometry histograms are shown in Fig. 4. Because the fluorescence intensity is proportional to the amount of DOX internalized by the cells, the mean fluorescence intensity was given to make a quantitative comparison of the endocytosis of DOX. For A549 cells treated with the equivalent DOX concentration in each formulation at the same incubation time (1 or 3 h), DOX-NP showed a little higher fluorescence intensity than free DOX. According to the literature, free DOX and DOX-NP had different cellular uptake methods [22]. Free DOX was transported into cells via a passive diffusion mechanism and could quickly diffuse through the cell membrane, while DOX-NP were taken up via the endocytosis pathway. This result indicated that DOX-NP had a higher cellular uptake by the endocytosis process.

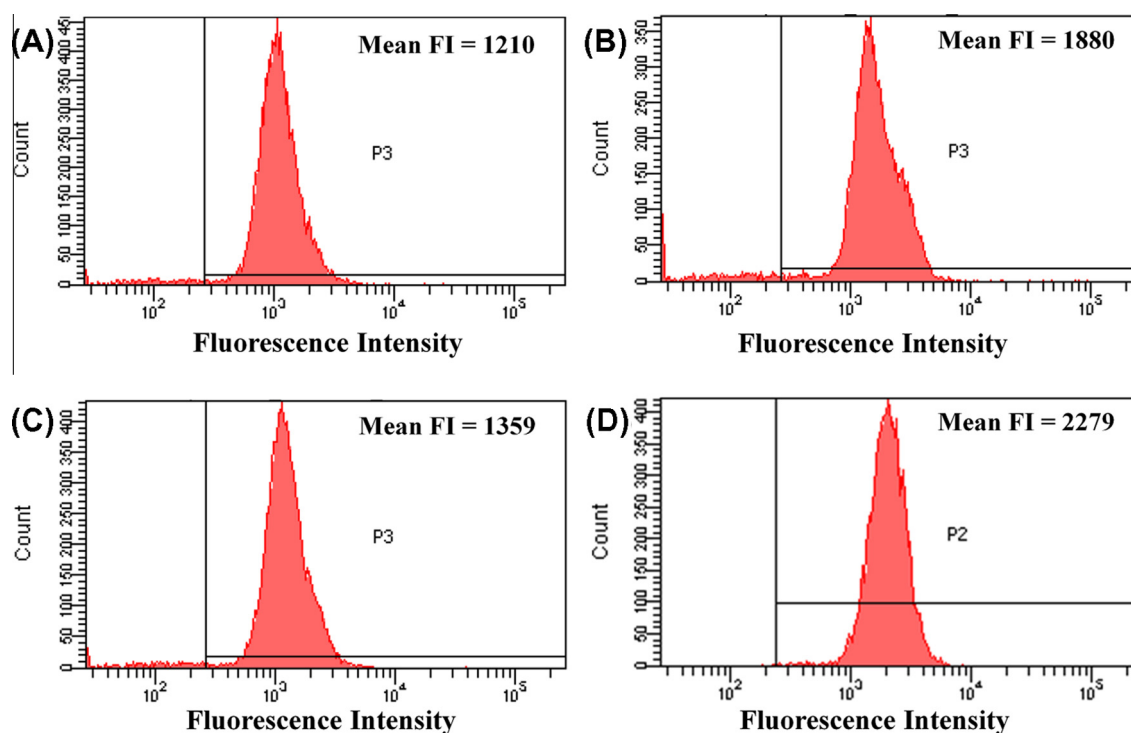


Fig. 4. Cell uptake of free DOX and DOX-NP after incubation with A549 cells for 1 h and 3 h by FACS (FI represents fluorescence intensity): (A) free DOX, 1 h; (B) DOX-NP, 1 h; (C) free DOX, 3 h; (D) DOX-NP, 3 h.

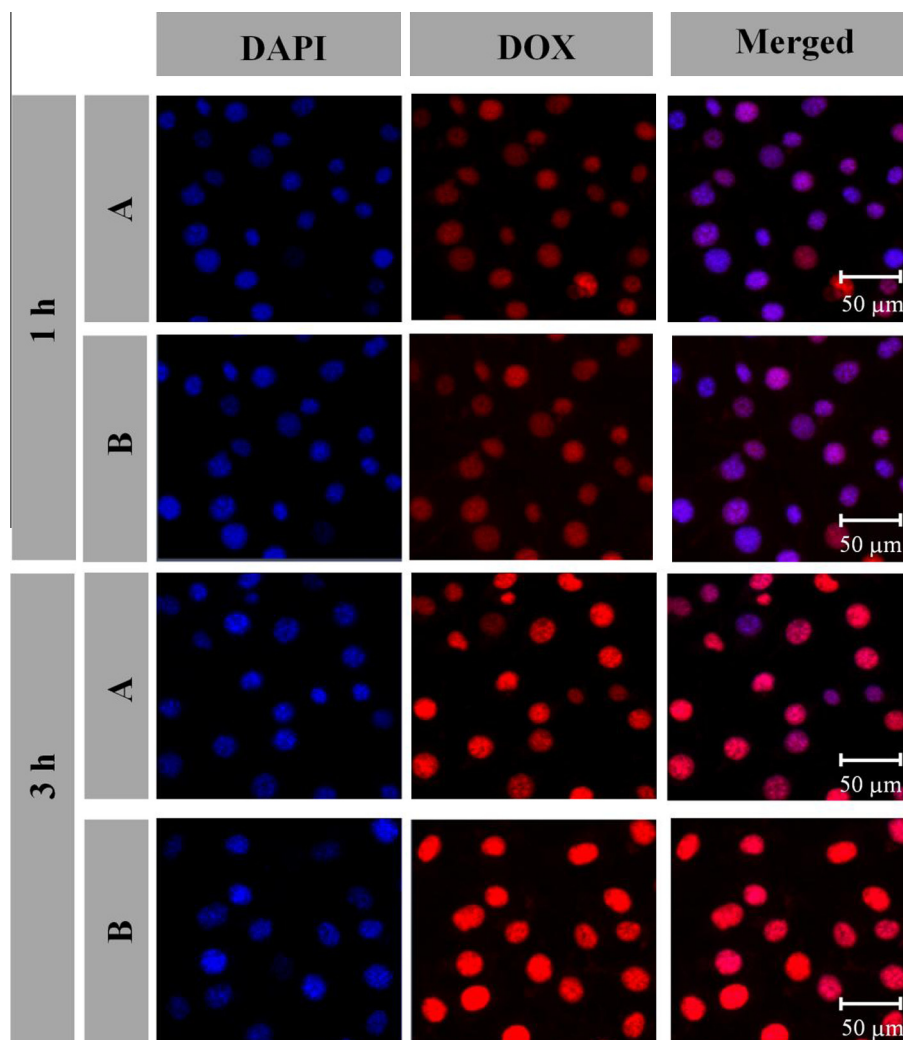


Fig. 5. Confocal laser scanning microscopy observation of A549 cells after incubation with (A) free DOX and (B) DOX-NP for 1 and 3 h.

The cellular uptake and intracellular distribution of free DOX and DOX-NP were further investigated using CLSM (Fig. 5). For both free DOX and DOX-NP, time-dependent cellular uptake was observed, since much higher fluorescence intensity was seen at 3 h than that at 1 h. Fig. 5 shows that free DOX was mostly distributed in the nuclei. However, DOX fluorescence was observed both in cytoplasm and nucleus for DOX-NP at both 1 and 3 h. DOX accumulation in both cytoplasm and nucleus for DOX-NP was slightly higher than that for free DOX at 1 and 3 h, which was consistent with the flow cytometry analysis. The DOX accumulation in the nucleus for free DOX occurred because the intracellular DOX molecules could pass quickly through the cell membrane to the cytosol and be rapidly transported to the nucleus and avidly bound to the chromosomal DNA. In the case of DOX-NP, DOX fluorescence was observed in both cytoplasm and nucleus, indicating that the DOX-NP were initially located within the intracellular compartments (endosomes and lysosomes), releasing DOX in a fast manner promoted by the increased acidity in subcellular compartments.

The in vitro cytotoxicity of mPEG-*b*-P(Glu-*co*-Phe) copolymer was evaluated using MTT assay. Two cell lines, HeLa (human cervical cancer) and A549 (human lung adenocarcinoma) cells were applied. As shown in Fig. 6A and B, the viability of HeLa and A549 cells treated with mPEG-*b*-P(Glu-*co*-Phe) was ~80–100% at all test concentrations up to 500 $\mu\text{g ml}^{-1}$, revealing the low toxicity and good compatibility of copolymer to cells.

The in vitro antitumor activity of DOX-loaded nanoparticles was also studied in HeLa and A549 cells. The cell viabilities were evaluated after 24 or 48 h incubation with DOX-NP, and free DOX was used as control. As shown in Fig. 6C and D, DOX-NP exhibited dose- and time-dependent cell proliferation inhibition for both HeLa and A549 cells. The results also show that DOX-NP appear to induce higher antitumor effect compared with free DOX. For HeLa cells, ic_{50} (i.e., inhibitory concentration to produce 50% cell death) of DOX-NP was determined as 1.15 and 0.40 $\mu\text{g ml}^{-1}$ after 24 or 48 h incubation time, respectively, which were lower than those observed for free DOX (1.80 and 0.57 $\mu\text{g ml}^{-1}$ after 24 or 48 h incubation time, respectively). A similar result was observed in A549 cells (1.50 and 0.64 $\mu\text{g ml}^{-1}$ for DOX-NP after 24 or 48 h incubation time, respectively, lower than those of 2.35 and 1.03 $\mu\text{g ml}^{-1}$ for free DOX after 24 or 48 h incubation time, respectively). The higher ic_{50} value of A549 cells compared with HeLa cells is consistent with the results in the literature that the NSCLC lines showed relative non-sensitivity to anticancer drugs [43].

The apoptotic activities of free DOX and DOX-NP on A549 cells were further evaluated by flow cytometry. Cells were double stained for viability (negative for PI) and apoptosis (positive for Annexin V-FITC). After incubated with the cells at a DOX concentration of 1 $\mu\text{g ml}^{-1}$ for 24 h, free DOX and DOX-NP resulted in 3.4 and 4.2% early apoptotic cells, 5.4 and 8.8% late apoptotic cells,

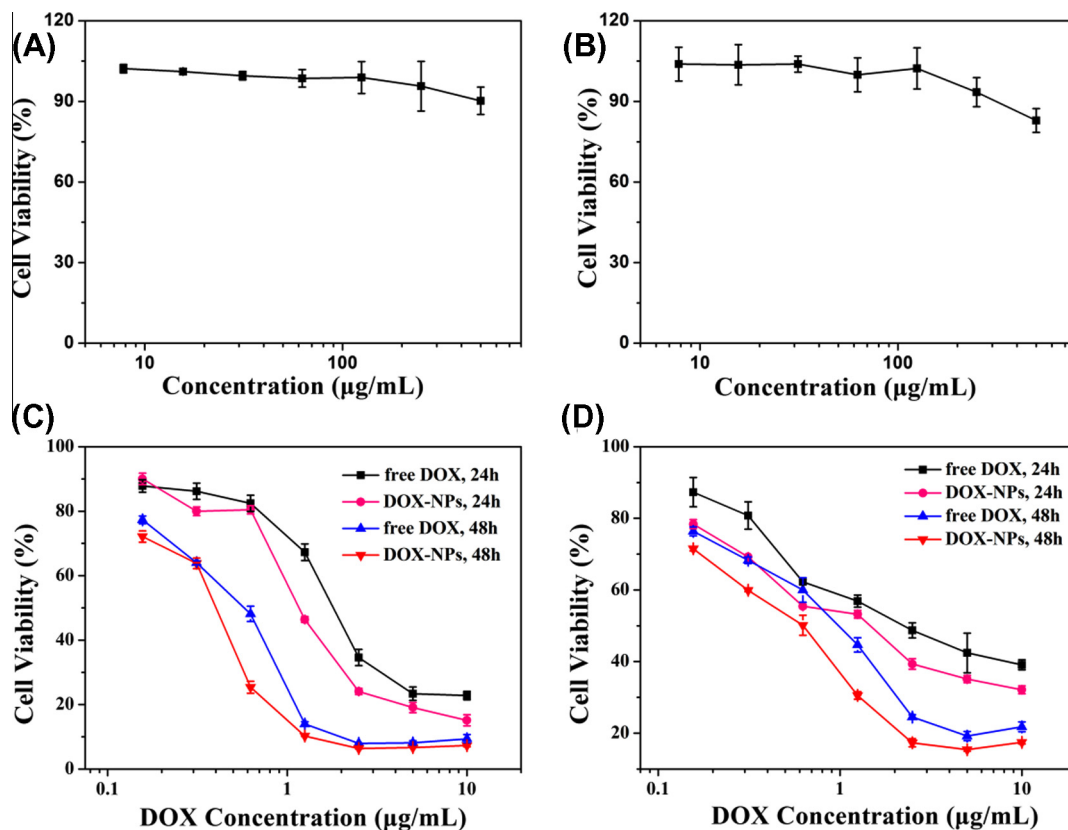


Fig. 6. In vitro cytotoxicity studies of mPEG-*b*-P(Glu-co-Phe), DOX and DOX-NP to HeLa and A549 cells by MTT assay. (A) In vitro cytotoxicities of mPEG-*b*-P(Glu-co-Phe) to HeLa cells for 48 h. (B) Cytotoxicities of mPEG-*b*-P(Glu-co-Phe) to A549 cells for 48 h. (C) Cytotoxicities of free DOX and DOX-NP to HeLa cells for 24 h and 48 h. (D) Cytotoxicities of free DOX and DOX-NP to A549 cells for 24 h and 48 h. Data are presented as mean \pm SD ($n = 3$).

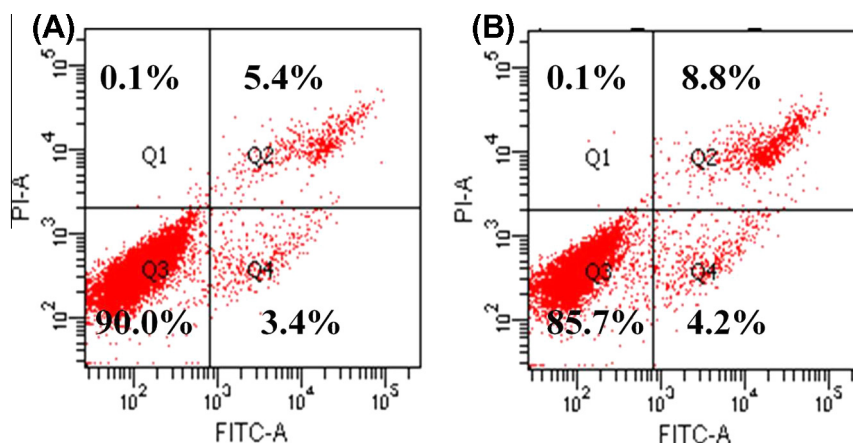


Fig. 7. Effect of (A) free DOX and (B) DOX-NP ($1 \mu\text{g ml}^{-1}$ DOX equivalent for 24 h) on A549 cell death and apoptosis as determined by FACS with PI and Annexin V-FITC staining.

and 90 and 85.7% normal cells, respectively (Fig. 7). Similarly to MTT assay (Fig. 5), the tendency towards an increased apoptotic activity of DOX-NP is probably due to the high level of cell uptake through endocytosis and a fast DOX release rate during the endocytosis process.

The stability of nanocarriers was found to be the key to a successful drug delivery system. The uptake of the drug carrier by tumor cells can be significantly enhanced with increasing stability, which further leads to a substantial increase in antitumor activity [28,29]. Previously, the present authors prepared a DOX-loaded

mPEG-*b*-PLG system in the therapy of NSCLC [27]. However, high hydrophilicity of both PEG and PLG segments in the block copolymer led to poorer cellular uptake and lower cell proliferation inhibition activity compared with free DOX-HCl. Compared with the present authors' former system, the above results confirmed that the present DOX-loaded mPEG-*b*-P(Glu-co-Phe) complex nanoparticles had a higher cell uptake level and better antitumor activity, which was attributed to the enhanced construct stability of DOX-NP by incorporation of phenylalanine into the mPEG-*b*-P(Glu-co-Phe) copolymer.

3.5. MTD study

The MTD for a single dose of DOX-NP was assessed in tumor-free Kunming mice and compared with free DOX. The mice were administered intravenously with different doses of DOX-NP or free DOX, followed by daily body weight measurement and observation of toxic death. As shown in Fig. 8, free DOX was well tolerated at the dose of 5 mg kg^{-1} . However, increasing DOX dosage to 10 mg kg^{-1} resulted in the death of two of the three treated mice, which was consistent with literature results that LD_{50} of DOX (the lethal dose for killing 50% of the test animals within a designated period) is $\sim 12 \text{ mg kg}^{-1}$ [44]. In contrast, there was only 10% body weight loss and no toxic death for the mice treated with DOX-NP at a DOX dosage as high as 15 mg kg^{-1} . From the present study, it can be estimated that the single i.v. MTD for free DOX was $\sim 5 \text{ mg kg}^{-1}$, while that for DOX-NP was $\sim 15 \text{ mg kg}^{-1}$. The high MTD for DOX-NP may be attributed to the slow release kinetics of DOX under physiological conditions (Fig. 3), the low levels of non-selective uptake by major normal organs (see below), and the remarkable biocompatibility and safety of the mPEG-*b*-P(Glu-co-Phe) block copolymer.

3.6. Excised imaging

To estimate the biodistribution of free DOX and DOX-NP, ex vivo DOX fluorescence images of the major organs (heart, liver, spleen, lung, kidney) and tumors at 2 h and 10 h post-injection were observed in A549 tumor-bearing nude mice, and the results are shown in Fig. 9. For the free DOX group, the liver and kidney showed the strongest DOX fluorescence at 2 h post-injection, and DOX fluorescence in kidney and tumor both became slightly weakened at 10 h post-injection as detected. The results suggest that,

while the free drug molecules were rapidly distributed in the body, they were captured mainly in the host defense and metabolic organs such as liver and kidney as foreign bodies, and metabolized or rapidly excreted by these organs, so leading to severe organ damage and low drug efficacy. In contrast, weaker fluorescence in the liver and stronger fluorescence in the tumor were observed at 2 and 10 h post-injection of DOX-NP compared with that of free DOX, indicating that DOX-NP could significantly alter the biodistribution of the drug and contribute to reduced toxicity and improved drug efficacy. In addition, DOX fluorescence in the tumor at 10 h post-injection became slightly stronger compared with that at 2 h post-injection for the DOX-NP group, suggesting that DOX-NP exhibited longer blood circulation and less uptake by the RES. The improved delivery of DOX to the tumors and the minimal uptake by RES system of DOX-NP were mainly due to the unusual PEG shielding effect, excellent stability of the polymer/drug formulation in the blood circulation, and the negative surface charge of the nanoparticles.

3.7. In vivo antitumor efficacy

To evaluate the antitumor activity of DOX-NP, efficacy studies were performed in mice bearing NSCLC A549 xenografts. Fourteen days after inoculation with A549 cells, mice were treated with free DOX and DOX-NP at 2 and 4 mg kg^{-1} DOX equivalents for a total of four doses via the tail vein. PBS was used as a control. The tumor volumes and the body weights were measured.

The changes in tumor volume and body weight are shown in Fig. 10. As shown in Fig. 10A, the tumor volumes in the control group (PBS) increased rapidly to $>1000 \text{ mm}^3$ in 17 days, and all DOX treatment groups decreased tumor growth rates ($p < 0.01$) compared with the control group. With the increase in DOX dose,

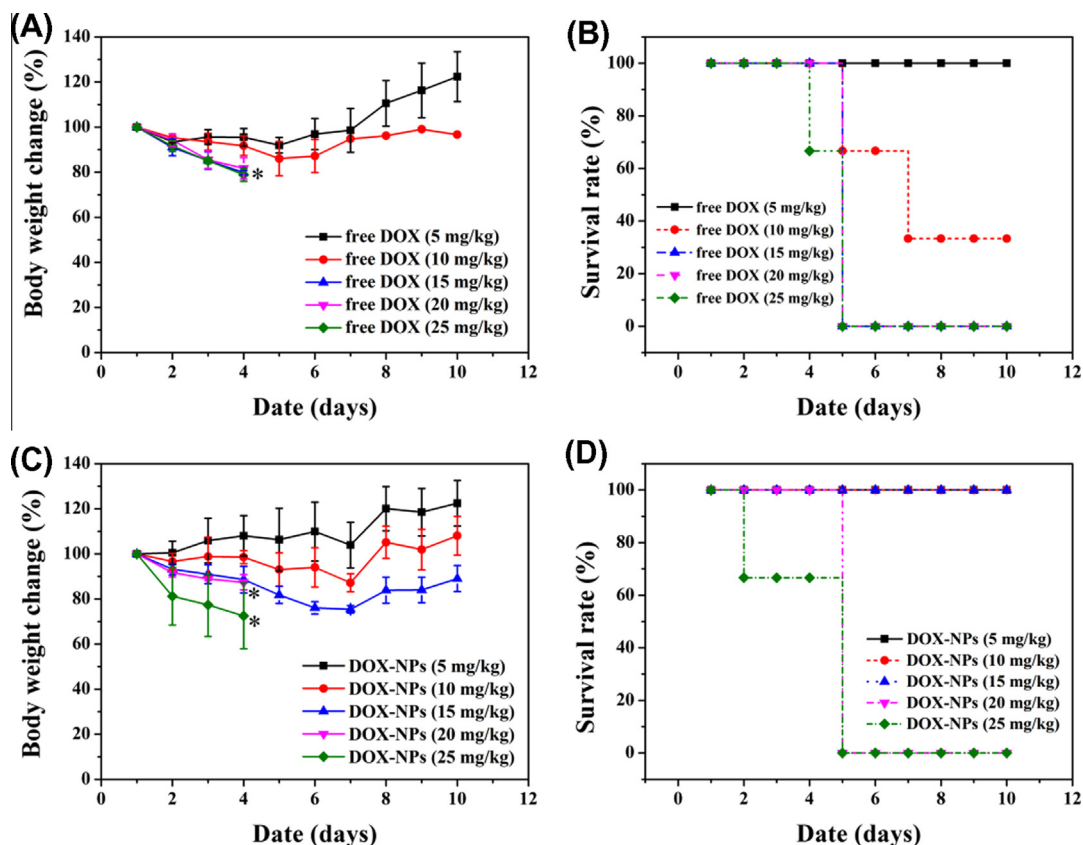


Fig. 8. MTD studies for free DOX and DOX-NP on body weight change and survival rate in tumor-free Kunming mice: (A, B) body weight change and survival rate for free DOX; (C, D) body weight change and survival rate for DOX-NP.

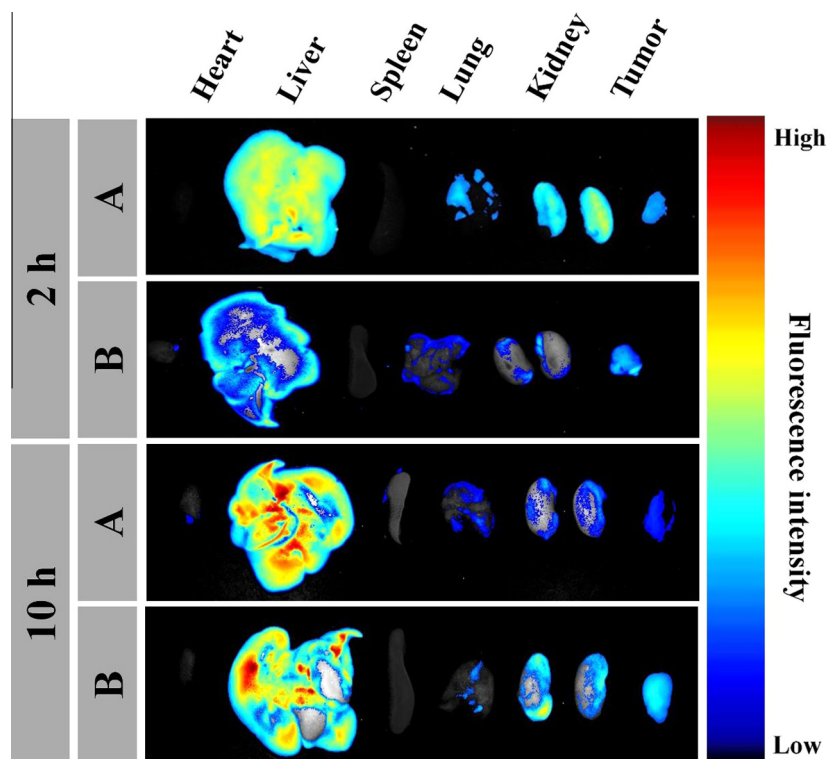


Fig. 9. Ex vivo DOX fluorescence images showing the drug bio-distribution of (A) free DOX and (B) DOX-NP in A549 tumor-bearing nude mice at 2 h and 10 h post-injection.

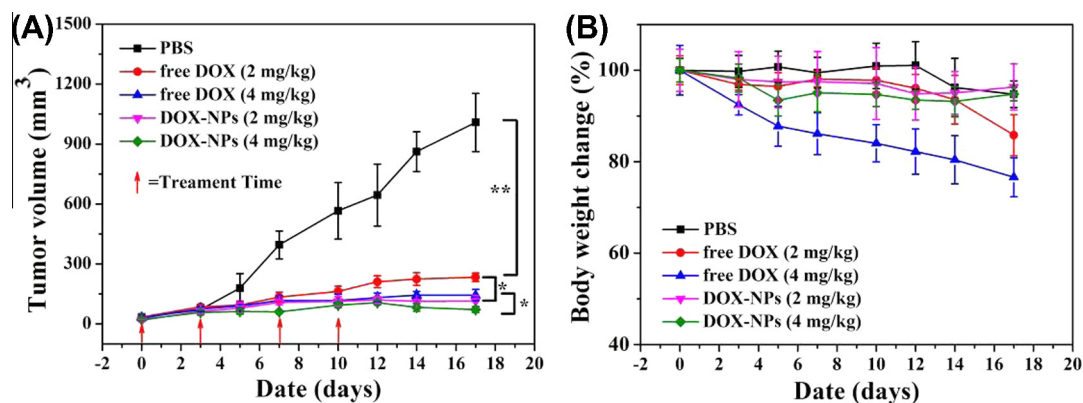


Fig. 10. Effect of DOX equivalents on anti-tumor efficacy in term of (A) tumor volume and (B) body weight change in A549 human lung cancer xenograft-bearing nude mice. The data are shown as mean \pm SD ($n = 6$), * $p < 0.05$, ** $p < 0.01$.

higher antitumor activities were observed in both free DOX and DOX-NP groups. In addition, the mice treated with DOX-NP had a significantly lower mean tumor volume ($p < 0.05$) than the mice in the free DOX groups at the same dose. For example, 17 days after injection, the average tumor volume in the free DOX and DOX-NP treated mice at 2 mg kg⁻¹ had reached 233 and 113 mm³, respectively, whereas the average tumor volume in the free DOX and DOX-NP treated mice at 4 mg kg⁻¹ was 143 and 72 mm³, respectively. Compared with the initial tumor volumes (~ 50 mm³), the tumor volumes barely increased in DOX-NP treated mice at 4 mg kg⁻¹, indicating that DOX-NP were significantly efficacious in the tumor reduction. The body weight loss is an important indicator for evaluating drug-related toxicity. As shown in Fig. 10A, treatment with free DOX at 4 mg kg⁻¹ resulted in the greatest body weight loss (24%) compared with free DOX at 2 mg kg⁻¹ (14%), which revealed that free drug had significant treatment-related

toxicities. In contrast, the treatment with DOX-NP at 2 or 4 mg kg⁻¹ appeared to be well tolerated and caused almost no decrease in body weight.

The above results demonstrated that DOX-NP exhibited enhanced antitumor activity over free DOX in terms of the tumor volume regression and greatly reduced the toxicity of DOX. One reason for the enhanced in vivo antitumor efficacy might be the enhanced accumulation at the tumor site of the DOX-NP, due to the EPR effect. In addition, the fast release of DOX from DOX-NP at the tumor site may contribute to the enhanced antitumor efficacy.

3.8. Histological and immunohistochemical analyses

To further confirm the anti-tumor efficacy of various DOX formulations, A549 tumor-bearing nude mice were sacrificed at the

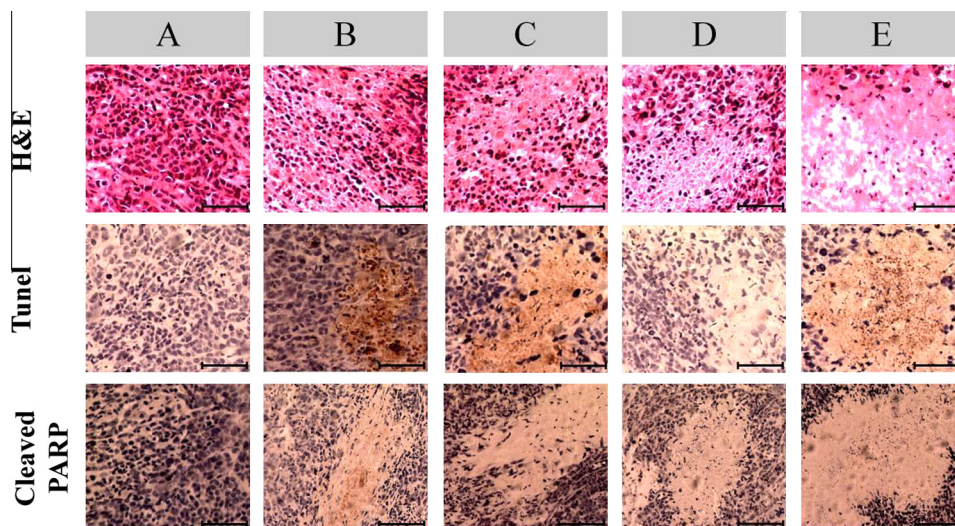


Fig. 11. Histopathological analysis of tumors in A549 human lung cancer xenograft-bearing nude mice: (A) PBS; (B) free DOX (2 mg kg^{-1}); (C) DOX-NP (2 mg kg^{-1}); (D) free DOX (4 mg kg^{-1}); (E) DOX-NP (4 mg kg^{-1}). Nuclei were stained bluish violet, while extracellular matrix and cytoplasm were stained pink in H&E staining. Brown and blue stains indicated apoptotic and normal cells, respectively, in TUNEL analysis; brown and blue stains indicated cleaved PARP1 and nuclei, respectively, in immunohistochemical assay. Scale bars: $200 \mu\text{m}$.

end of the treatment, and the tumor sections were prepared for pathology analysis (Fig. 11).

By H&E staining, nuclei were stained blue by hematoxylin, while cytoplasm and extracellular matrix were stained pink by eosin in normal tissues. However, necrotic cells did not have a clear cell morphology; and the chromatin became darker or diffused separately extracellularly, and the nuclei became pyknotic or absence. As shown in the figure, tumor cells with clear cell morphology and more chromatin and binucleolates were observed in the PBS group. The tumor tissues treated with all DOX formulations showed various degrees of necrosis, indicating that all DOX formats applied had the obvious antitumor effect on A549 lung cancer. For both free DOX and DOX-NP, the level of tissue necrosis was improved as the DOX dose increased. At the same DOX dose, the tumor tissue treated with DOX-NP showed higher damage compared with that treated with free DOX. Among all the treated groups, DOX-NP at the 4 mg kg^{-1} dose showed the most distinct damage to tumor tissues, as much nuclei absence and lack of discernible boundary regions were observed, and the above result was consistent with *in vivo* tumor growth inhibition study. A TUNEL assay further demonstrated the degree of apoptosis induced by various formulations. As shown in Fig. 11, little apoptosis was observed in tumor tissues treated by PBS. However, obvious cell apoptosis was detected in all DOX formulation treated groups. DOX-NP also induced more cellular apoptosis compared with free DOX at the same dose, and the treatment of DOX-NP at a dose of 4 mg kg^{-1} showed the highest level of cell apoptosis in the tumor tissue, which was consistent with H&E observation.

PARP, one of the essential substrates cleaved by both caspase-3 and caspase-7, is an abundant DNA-binding enzyme that detects and signals DNA strand breaks. The presence of cleaved PARP1 is one of the diagnostic tools most used to detect apoptosis in many cell types. The present study assessed apoptosis using PARP to further confirm the tumor apoptosis: the cleaved 25 kDa fragment of PARP1 was analyzed in the tumor sections by immunohistochemistry. As shown in Fig. 11, the cleavage products were detected in the sections of tumor tissues treated with all DOX formulations, and the more positive signals could be found in DOX-NP treated tumors compared with free DOX treated ones at the same dose, indicating that DOX-NP led to more cell apoptosis in the tumor tissues compared with free DOX.

4. Conclusions

The present authors developed an effective drug delivery system based on an anionic mPEG-*b*-P(Glu-*co*-Phe) block copolymer and a model cationic anticancer drug, DOX. The block copolymer exhibited excellent biocompatibility, convenient fabrication, robust self-assembling structure under the physiological conditions, a high drug-loading capability and an intracellular pH-triggered drug release capability, revealing its great potential for delivering anticancer drugs. The CLSM and flow cytometry assays showed that DOX-NP had a high level of tumor cell uptake compared with free DOX. The *in vitro* cytotoxicity and the cell apoptosis studies confirmed that DOX-NP exhibited higher tumor cell growth inhibition over free DOX. When administered *in vivo*, DOX-NP had an excellent safety profile, with MTD of $15 \text{ mg DOX kg}^{-1}$, which was higher than that (5 mg DOX kg^{-1}) for free DOX. The *in vivo* studies on A549 lung-tumor-bearing mice demonstrated that DOX-NP exhibited increased tumor accumulation, reduced toxicity and higher antitumor efficacy compared with free DOX at the same dose. Thus, the self-assembled polymer/drug complexes driven by electrostatic interactions may be a promising drug delivery system for cancer therapy.

Acknowledgements

This work was supported by grants from the National Natural Science Foundation of China (51173184, 21104076, 51233004, 51021003), the Ministry of Science and Technology of China (2011DFR51090) and the Knowledge Innovation Program of the Chinese Academy of Sciences (Grant No. KJCX2-YW-H19). The authors have declared no conflict of interest.

Appendix A. Figures with essential colour discrimination

Certain figures in this article, particularly Figs. 3–11, are difficult to interpret in black and white. The full colour images can be found in the on-line version, at doi: <http://dx.doi.org/10.1016/j.actbio.2013.08.015>.

References

- [1] Nam K, Nam HY, Kim PH, Kim SW. Paclitaxel-conjugated PEG and arginine-grafted bioreducible poly (disulfide amine) micelles for co-delivery of drug and gene. *Biomaterials* 2012;33:8122–30.
- [2] Uchino H, Matsumura Y, Negishi T, Koizumi F, Hayashi T, Honda T, et al. Cisplatin-incorporating polymeric micelles (NC-6004) can reduce nephrotoxicity and neurotoxicity of cisplatin in rats. *Br J Cancer* 2005;93:678–87.
- [3] Kurzrock R, Goel S, Wheler J, Hong D, Fu S, Rezaei K, et al. Safety, pharmacokinetics, and activity of EZN-2208, a novel conjugate of polyethylene glycol and SN38, in patients with advanced malignancies. *Cancer* 2012;118:6144–51.
- [4] Miyata K, Christie RJ, Kataoka K. Polymeric micelles for nano-scale drug delivery. *React Funct Polym* 2011;71:227–34.
- [5] Shah NB, Vercellotti GM, White JG, Fegan A, Wagner CR, Bischof JC. Blood-nanoparticle interactions and in vivo biodistribution: impact of surface PEG and ligand properties. *Mol Pharm* 2012;9:2146–55.
- [6] Bae YH, Park K. Targeted drug delivery to tumors: myths, reality and possibility. *J Controlled Release* 2011;153:198–205.
- [7] Wei H, Zhang XZ, Chen WQ, Cheng SX, Zhuo RX. Self-assembled thermosensitive micelles based on poly(L-lactide-star block-N-isopropylacrylamide) for drug delivery. *J Biomed Mater Res, Part A* 2007;83:980–9.
- [8] de Graaf AJ, dos Santos IAP, Pieters EHE, Rijkers DTS, van Nostrum CF, Vermonden T, et al. A micelle-shedding thermosensitive hydrogel as sustained release formulation. *J Controlled Release* 2012;162:582–90.
- [9] Xiaoming Z, Tao J, Feng HE. Synthesis and characterization of PNIPAM-b-polycarbonate copolymers as self-assembled thermosensitive micelles for drug delivery. *Acta Polym Sin* 2011;895–902.
- [10] Chen W, Meng FH, Cheng R, Zhong ZY. pH-sensitive degradable polymersomes for triggered release of anticancer drugs: a comparative study with micelles. *J Controlled Release* 2010;142:40–6.
- [11] Ko J, Park K, Kim Y-S, Kim MS, Han JK, Kim K, et al. Tumoral acidic extracellular pH targeting of pH-responsive MPEG-poly(β -amino ester) block copolymer micelles for cancer therapy. *J Controlled Release* 2007;123:109–15.
- [12] Song W, Tang Z, Li M, Lv S, Yu H, Ma L, et al. Tunable pH-sensitive poly(β -amino ester)s synthesized from primary amines and diacrylates for intracellular drug delivery. *Macromol. Biosci.* 2012;12:1375–83.
- [13] Wei R, Cheng L, Zheng M, Cheng R, Meng F, Deng C, et al. Reduction-responsive disassemblable core-cross-linked micelles based on poly(ethylene glycol)-*b*-poly(*N*-2-hydroxypropyl methacrylamide)-lipoic acid conjugates for triggered intracellular anticancer drug release. *Biomacromolecules* 2012;13:2429–38.
- [14] Li M, Tang Z, Sun H, Ding J, Song W, Chen X. PH and reduction dual-responsive nanogel cross-linked by quaternization reaction for enhanced cellular internalization and intracellular drug delivery. *Polym Chem* 2013;4:1199.
- [15] Barenholz Y. Doxil (R) – the first FDA-approved nano-drug: lessons learned. *J Controlled Release* 2012;160:117–34.
- [16] Gradishar WJ, Tjulandin S, Davidson N, Shaw H, Desai N, Bhar P, et al. Phase III trial of nanoparticle albumin-bound paclitaxel compared with polyethylated castor oil-based paclitaxel in women with breast cancer. *J Clin Oncol* 2005;23:7794–803.
- [17] Bae Y, Kataoka K. Intelligent polymeric micelles from functional poly(ethylene glycol)-poly(amino acid) block copolymers. *Adv Drug Deliv Rev* 2009;61:768–84.
- [18] Shiraiishi K, Hamano M, Ma HL, Kawano K, Maitani Y, Aoshi T, et al. Hydrophobic blocks of PEG-conjugates play a significant role in the accelerated blood clearance (ABC) phenomenon. *J Controlled Release* 2013;165:183–90.
- [19] Wang K, Luo GF, Liu Y, Li C, Cheng SX, Zhuo RX, et al. Redox-sensitive shell cross-linked PEG-polypeptide hybrid micelles for controlled drug release. *Polym Chem* 2012;3:1084–90.
- [20] Tian Z, Wang M, Zhang A-y, Feng Z-g. Preparation and evaluation of novel amphiphilic glycopeptide block copolymers as carriers for controlled drug release. *Polymer* 2008;49:446–54.
- [21] Prompruk K, Govender T, Zhang S, Xiong CD, Stolnik S. Synthesis of a novel PEG-block-poly(aspartic acid-stat-phenylalanine) copolymer shows potential for formation of a micellar drug carrier. *Int J Pharm* 2005;297:242–53.
- [22] Prabakaran M, Grailler JJ, Pilla S, Steeber DA, Gong S. Amphiphilic multi-arm-block copolymer conjugated with doxorubicin via pH-sensitive hydrazone bond for tumor-targeted drug delivery. *Biomaterials* 2009;30:5757–66.
- [23] Matsumura Y, Hamaguchi T, Ura T, Muro K, Yamada Y, Shimada Y, et al. Phase I clinical trial and pharmacokinetic evaluation of NK911, a micelle-encapsulated doxorubicin. *Br J Cancer* 2004;91:1775–81.
- [24] Hamaguchi T, Kato K, Yasui H, Morizane C, Ikeda M, Ueno H, et al. A phase I and pharmacokinetic study of NK105, a paclitaxel-incorporating micellar nanoparticle formulation. *Br J Cancer* 2007;97:170–6.
- [25] Plummer R, Wilson RH, Calvert H, Boddy AV, Griffin M, Sludden J, et al. A phase I clinical study of cisplatin-incorporated polymeric micelles (NC-6004) in patients with solid tumours. *Br J Cancer* 2011;104:593–8.
- [26] Matsumura Y. Preclinical and clinical studies of NK012, an SN-38-incorporating polymeric micelles, which is designed based on EPR effect. *Adv Drug Deliv Rev* 2011;63:184–92.
- [27] Li M, Song W, Tang Z, Lv S, Lin L, Sun H, et al. Nanoscaled poly(L-glutamic acid)/doxorubicin-amphiphile complex as pH-responsive drug delivery system for effective treatment of nonsmall cell lung cancer. *ACS Appl Mater Interfaces* 2013;5:1781–92.
- [28] Huynh VT, Quek JY, de Souza PL, Stenzel MH. Block copolymer micelles with pendant bifunctional chelator for platinum drugs: effect of spacer length on the viability of tumor cells. *Biomacromolecules* 2012;13:1010–23.
- [29] Kim Y, Pourgholami MH, Morris DL, Stenzel MH. Effect of cross-linking on the performance of micelles as drug delivery carriers: a cell uptake study. *Biomacromolecules* 2012;13:814–25.
- [30] Oh KT, Oh YT, Oh NM, Kim K, Lee DH, Lee ES. A smart flower-like polymeric micelle for pH-triggered anticancer drug release. *Int J Pharm* 2009;375:163–9.
- [31] Akao T, Kimura T, Hirofujii Y-s, Matsunaga K, Imayoshi R, Nagao J-i, et al. A poly(γ -glutamic acid)-amphiphile complex as a novel nanovehicle for drug delivery system. *J Drug Target* 2010;18:550–6.
- [32] Manocha B, Margarithis A. Controlled release of doxorubicin from doxorubicin/ γ -polyglutamic acid ionic complex. *J Nanomater* 2010;2010:1–9.
- [33] Du YF, Chen W, Zheng M, Meng FH, Zhong ZY. pH-sensitive degradable chimaeric polymersomes for the intracellular release of doxorubicin hydrochloride. *Biomaterials* 2012;33:7291–9.
- [34] Huang WC, Chiang WH, Huang YF, Lin SC, Shih ZF, Chern CS, et al. Nano-scaled pH-responsive polymeric vesicles for intracellular release of doxorubicin. *J Drug Target* 2011;19:944–53.
- [35] Ding J, Zhuang X, Xiao C, Cheng Y, Zhao L, He C, et al. Preparation of photo-cross-linked pH-responsive polypeptide nanogels as potential carriers for controlled drug delivery. *J Mater Chem* 2011;21:11383.
- [36] Wang Z, Ho PC. A nanocapsular combinatorial sequential drug delivery system for antiangiogenesis and anticancer activities. *Biomaterials* 2010;31:7115–23.
- [37] Dai J, Lin S, Cheng D, Zou S, Shuai X. Interlayer-crosslinked micelle with partially hydrated core showing reduction and pH dual sensitivity for pinpointed intracellular drug release. *Angew Chem Int Ed Engl* 2011;50:9404–8.
- [38] Bressenot A, Marchal S, Bezdetnaya L, Garrier J, Guillemin F, Plenat F. Assessment of apoptosis by immunohistochemistry to active caspase-3, active caspase-7, or cleaved PARP in monolayer cells and spheroid and subcutaneous xenografts of human carcinoma. *J Histochem Cytochem* 2009;57:289–300.
- [39] Kataoka K, Harada A, Nagasaki Y. Block copolymer micelles for drug delivery: design, characterization and biological significance. *Adv Drug Deliv Rev* 2001;47:113–31.
- [40] Deng J, Gao N, Wang Y, Yi H, Fang S, Ma Y, et al. Self-assembled cationic micelles based on PEG-PLL-PLLeu hybrid polypeptides as highly effective gene vectors. *Biomacromolecules* 2012;13:3795–804.
- [41] Xiao K, Li Y, Luo J, Lee JS, Xiao W, Gonik AM, et al. The effect of surface charge on in vivo biodistribution of PEG-oligocholic acid based micellar nanoparticles. *Biomaterials* 2011;32:3435–46.
- [42] Du JZ, Sun TM, Song WJ, Wu J, Wang J. A tumor-acidity-activated charge-conversional nanogel as an intelligent vehicle for promoted tumoral-cell uptake and drug delivery. *Angew Chem Int Ed Engl* 2010;49:3621–6.
- [43] Tsai HY, Chiu CC, Lin PC, Chen SH, Huang SJ, Wang LF. Antitumor efficacy of doxorubicin released from crosslinked nanoparticulate chondroitin sulfate/chitosan polyelectrolyte complexes. *Macromol Biosci* 2011;11:680–8.
- [44] Bae Y, Nishiyama N, Fukushima S, Koyama H, Yasuhiro M, Kataoka K. Preparation and biological characterization of polymeric micelle drug carriers with intracellular pH-triggered drug release property: tumor permeability, controlled subcellular drug distribution, and enhanced in vivo antitumor efficacy. *Bioconjug Chem* 2005;16:122–30.